Noise Radiation Patterns of Counter-Rotation and Unsteadily Loaded Single-Rotation Propellers

P. J. W. Block*
NASA Langley Research Center, Hampton, Virginia

In order to understand the effects of installation on propeller noise, numerous measurements are required to define the directivity of the noise as well as the level. An experimental study was designed to map the noise radiation pattern for various single-rotation propeller (SRP) installations and one counter-rotation propeller (CRP) installation covering an area ±60 deg from the propeller disk plane and ±60 deg laterally. The configurations considered included an SRP at angle of attack and in tractor and pusher operations and a CRP. A first-principles linear theory was validated for the SRP tractor operation over the angle range mentioned above. The increases in noise that arise from an unsteady loading operation such as an SRP pusher or a CRP exceed 15 dB and depend on the observer location. In particular, the majority of the additional noise from the unsteady loading appears to radiate in the axial directions.

Introduction

RECENT studies have shown that turboprop aircraft offer significant fuel savings over turbofan aircraft. Therefore, new aircraft propulsion systems are incorporating new and advanced propeller concepts such as highly swept and tapered propeller blades mounted in pusher and counter-rotation configurations. However, the impact of these concepts on propeller noise radiation is of concern both from the cabin or interior noise standpoint and from that of the community. To assess the noise impact, near- and far-field propeller noise measurements are needed on advanced propeller installations. These measurements are needed to validate available prediction methods and to supplement the data base on advanced propeller installation effects.

Little data are available on the noise produced by a propeller operating in an installed environment, such as at an angle of attack α or in an airfoil wake (pusher installation) or for counter-rotation propellers. References 1-4 are examples of experimental studies aimed at understanding these installation effects. The results from Refs. 3 and 4 indicate that the noise produced by the unsteady loading, which arises in the installed environment, has strong directivity aspects requiring numerous measurements to define the directivity as well as the levels of the noise. The present paper addresses this area with an experimental study designed to define the noise radiation patterns for single-rotation propellers (SRP) in a representative set of installed propeller environments and for counter-rotation propellers (CRP). The SRP installations considered in this study include tractors at $\alpha = 0$ deg (baseline) and ± 8 deg, and a pylon-mounted pusher. The only CRP installation addressed here is sting-mounted tractor at 0 deg a-o-a. The propellers were of the straight-bladed SR-2 design. The test matrix was divided into two operating conditions—a lightly loaded high tip Mach number operation and a more heavily loaded low tip Mach number operation. A remotely controlled microphone carriage was used to map the noise radiation patterns over a square area extending from 60 deg in front of the propeller disk to 60 deg behind it and about 60 deg to either side of the propeller axis. The uninstalled configuration (SRP at $\alpha = 0$ deg) results are compared with levels predicted by Farassat's formulation[5,6] and the directional aspects of the installed configurations are presented.

Presented as Paper 84-2263 at the AIAA/NASA 9th Aeroacoustics Conference, Williamsburg, VA, Oct. 15-17, 1984; received Nov. 1, 1984; revision received May 2, 1985. This paper is declared a work of the U.S. Government and therefore is in the public domain.

*Aerospace Engineer, Acoustics Division. Member AIAA.

Description of the Experiment

Propellers

The entire experiment is described in detail in Ref. 7. The description given below covers those aspects pertaining to the set of data presented herein. The SR-2 propeller design was employed in this study. The coordinates[8] of this design are displayed in three-dimensional form in Fig. 1. The hubs for the SRP and CRP permitted two-, four-, or eight-blade operation over a blade pitch angle range of -2 to 60 deg. Both the SRP and CRP systems were driven by a single 29 hp, 10,000 rpm electric motor.

The SRP was 0.429 m (16.9 in.) in diameter and the blade pitch angles were adjustable in increments of 1 deg. The CRP was 0.409 m (16.1 in.) and its coordinates were obtained by scaling the SRP coordinates down by a factor of 0.88757 to a diameter of 0.381 m (15.0 in.). The blades were then shifted out radially 0.014 m (0.552 in.), which added 1.1 in. to the diameter. The hub for the CRP permitted a continuous range of blade angle settings. Each disk of the CRP had the same pitch setting and both rotated at the same rotational speed. For a 4+4 blade CRP, there are a set of eight azimuthal locations where the blades appeared to overlap to an observer standing in front of the propeller. These locations were spaced every 45 deg from 24 deg counterclockwise from the vertical looking downstream. The pitch change axes of the two rows of blades were separated by 2.31 in.

Nacelle, Strut, and Sting

The nacelle was a cylinder with a maximum outside diameter of 0.15 m (6.0 in.). All the test hardware configurations are shown schematically in Fig. 2.

There were two mounts for the nacelle—the sting mount in which the nacelle was an aerodynamic extension of the straight sting and the pylon or strut mount in which the nacelle was attached to a scaled horizontal tail surface extending from the sting via an adapter (see also Fig. 3). There were two configurations for the nacelle in the pylon mount—tractor (propeller precedes pylon) and pusher (propeller follows pylon).

The pylon was a tapered NACA 0012 airfoil. The chord length above the nacelle was 0.318 m (12.5 in.) and below the nacelle it was 0.254 m (10 in.).

The straight sting was used keep the height of the propeller axis 0.889 m (35.0 in.) above the microphone carriage for every configuration. The adapter, which connected the pylon to the sting, permitted the nacelle to be yawed in increments of

±5 deg, with the position of the centerline of the propeller disk held fixed.

Microphone Carriage

The microphone carriage was a streamlined rectangular flat plate holding an array of 11 flush-mounted microphones. (See Fig. 3.) It was designed to circumvent the complexity of reflections from the tunnel floor, while providing the capability of making numerous streamwise noise measurements of all the propeller configurations under a very small boundary layer of constant thickness.

The carriage was 1.8 m (72 in.) wide (streamwise), 4.27 m (168 in.) long (cross-stream dimension), and 0.0584 m (2.30 in.) thick. It had a rigid foam core and an aluminum skin bonded together with an epoxy adhesive. A sketch of the carriage showing the microphone locations is given in Fig. 4.

The carriage was moved in the streamwise direction on Thompson bearings and a set of 1 in. diameter stainless steel rods. (See Fig. 3.) The carriage was positioned at 13-15 fixed streamwise locations, which corresponded to nominal increments of 10 deg from the propeller disk plane, beginning at 60 deg in front of the disk plane and ending 60 deg behind for the reference condition. Two more stops were added for some of the CRP runs to measure the noise at 72 and 78 deg in front of the disk plane. Thus, the noise radiation pattern for each of the propeller configurations was measured at a minimum of 143 locations covering the range of ±60 deg streamwise and about 60 deg laterally.

Facility

The tests were conducted in the Langley 4×7 M Tunnel. This is a closed, single-return, atmospheric wind tunnel allowing open or closed test section operation. A more detailed description of this facility and an acoustic evaluation of the open test section (OTS) are given in Ref. 9. Figure 5 is a plan view scaled drawing showing the size of the OTS, the size of the microphone carriage, the array of microphones, the propeller plane location, and the locations of the acoustic treatment. The treatment consisted of open-cell foam bats 0.152 m (6 in.) thick applied to the raised ceiling, sidewalls, and control room wall. A tone burst calibration showed that within the dynamic range of the recording instrumentation, the microphone systems were not able to detect reflections from these surfaces.

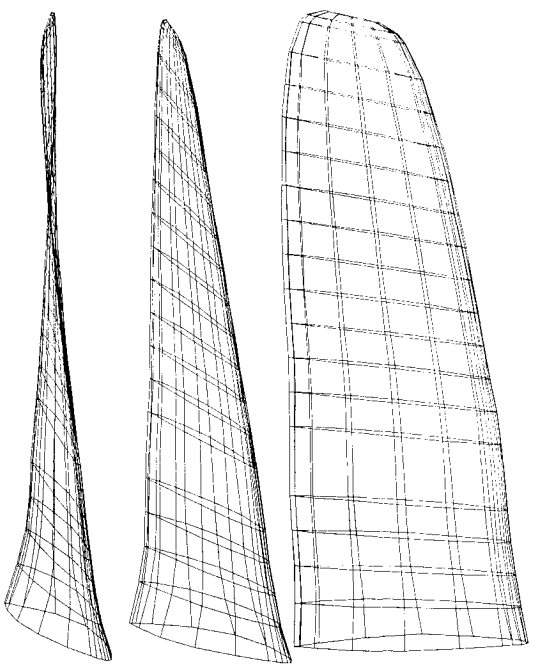

Fig. 1 Computer-generated three-dimensional display of SR-2 blade.

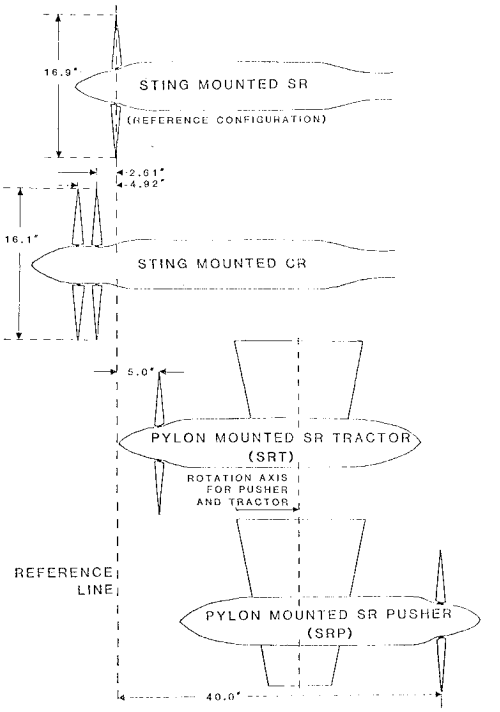

Fig. 2 Test hardware configurations.

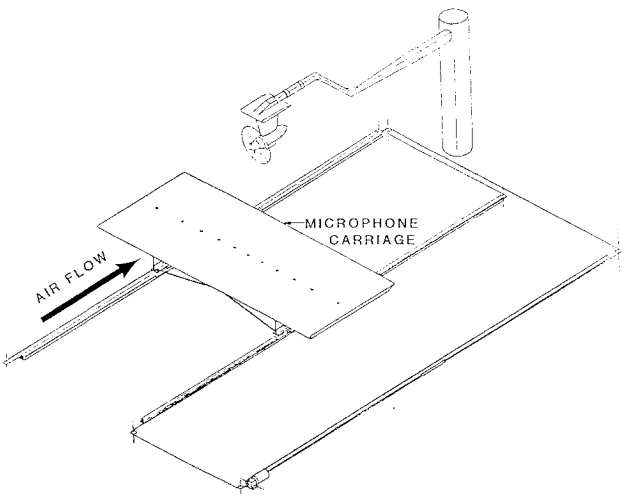

Fig. 3 Scaled isometric sketch of microphone carriage.

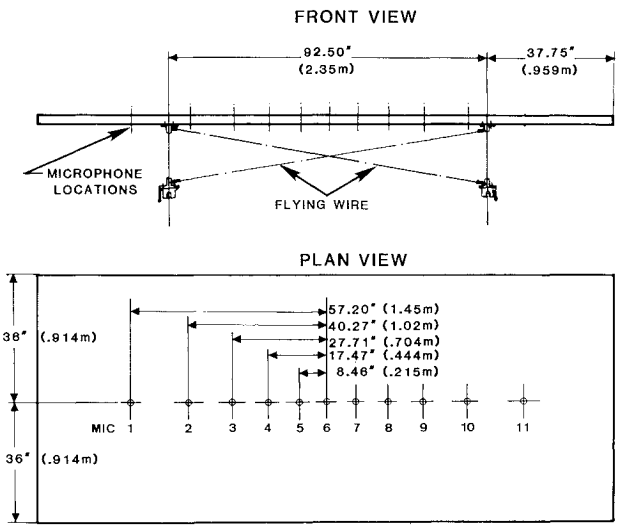

Fig. 4 Plan view and front view of microphone carriage.

Test Conditions

Table 1 gives the conditions at which the data were acquired in this test. All data were obtained at a tunnel dynamic pressure of 575 Pa (1216/ft^2), which gave a nominal tunnel speed of 30.8 m/s (101 ft/s).

The SR and CR propellers were each tested with four blades per disk or per row (see column 5 of Table 1). An eight-blade SRP was also tested to provide a comparison with the two four-blade CRPs in which the total number of blades is the same.

The propeller pitch and rotational speeds were chosen to emphasize either the thickness noise or the loading noise. At a high rotational tip speed of 743 ft/s (168 rev/s), a blade angle $\beta_{0.75}$ of 13 deg was chosen because it represented the most efficient operation of the propeller at a tunnel speed of 101 ft/s. Similarly, 21 deg was chosen for the lower rotation speed of 442 ft/s (100 rev/s). At each blade setting $\beta_{0.75}$, an additional (higher) rotational speed was examined to increase the loading and tip speed of the propeller without stalling it (see columns 6 and 7 of Table 1).

To examine the effect of simply changing the pitch of the propeller shaft or axis, the noise of the sting-mounted SRP and CRP was mapped at $\alpha = -8$, 0, and 8 deg. For these runs the height of the propeller was held at 0.889 m (35.0 in.) above the microphone carriage; however, the axial location did shift slightly.[7] The propeller axis was also yawed 10 deg with the center of the disk kept at the same location (see columns 8 and 9).

The axial force (propeller thrust at 0 deg a-o-a) is given in the last column of Table 1.

Data Reduction and Presentation

The microphone data were high-pass filtered at 80 Hz and FM recorded on 1 in. magnetic tape at 60 in./s. A triple-redundancy system was employed for recording the attenuator settings. A once-per-revolution pulse, which was generated by a magnetic sensor on the shaft, was also recorded. The recorded data were digitized using the once-per-revolution pulse to obtain 512 points of data for each revolution of the shaft. A minimum of 120 revolutions of data were stored for each microphone (61,440 points) for averaging.

The data were analyzed in the time and the frequency domains. The data presented herein were analyzed in the frequency domain by the following method. Each revolution of data was Fourier analyzed to produce the sine and cosine coefficients for the first 25 harmonics of the blade passage frequency (BPF) (a_n and b_n, respectively, $n = 1, 2, \ldots, 25$). These coefficients were averaged over the 120 revolutions of data to yield $\bar{a}_n$ and $\bar{b}_n$. The rms amplitude of the noise contribution

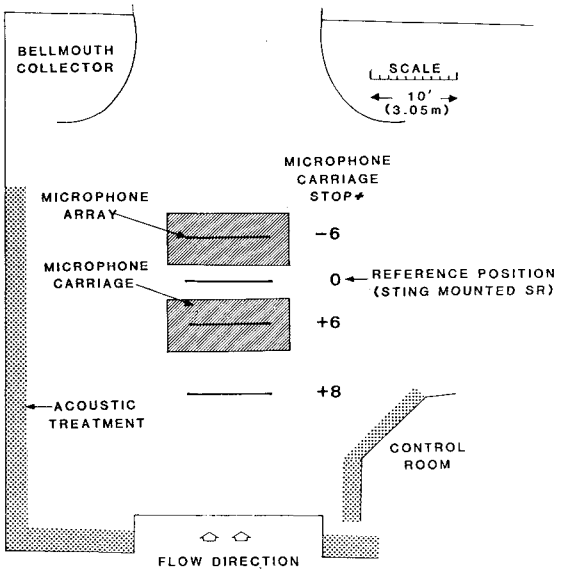

Fig. 5 Plan view of the Langley 4×7 M Tunnel open test section.

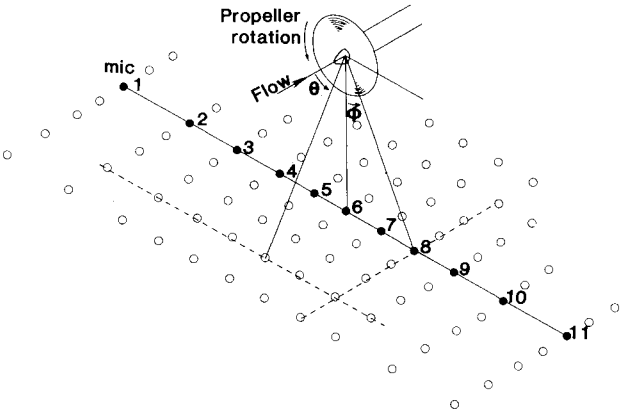

Fig. 6 Coordinate system for data comparisons.

Table 1 Configuration description and test conditions

Runs	Mount	Config.	Prop. type	No. of blades	$\beta_{0.75}$, deg[a]	Speed, rev/s	Nacelle attitude, deg Pitch	Nacelle attitude, deg Yaw	Axial force, lbf
52, 53	Sting	Tractor	SR	4	20.6	100, 120	0	0	17.7, 26.4
54, 55					12.7	168, 190			[b] [b]
63, 64					20.6	100, 120	8	0	6.0, 15.5
65, 66							−8		6.3, 16.1
67, 68					12.7	168, 190	8		16.8, 27.5
69, 70						190, 168	−8		28.6, 17.8
82, 83			CR	4+4	21.3	100, 120	0	0	9.8, 21.9
84, 85					13.3	168, 190			25.5, 39.3
132, 133	Pylon	Pusher	SR	4	12.7	168, 190	0	0	15.0, 26.2
134, 135					20.6	100, 120			14.1, 25.8
141, 142		Tractor	SR	8	12.7	168, 190	0	0	20.6, 34.8
144, 145				4	12.7	168, 190			15.4, 26.3
147, 148					12.7	168, 190		10	12.9, 23.0
150, 151					20.6	100, 120			4.4, 13.2

[a] Propeller pitch setting at 0.75 radial station with respect to the plane of rotation. [b] Balance data in question.

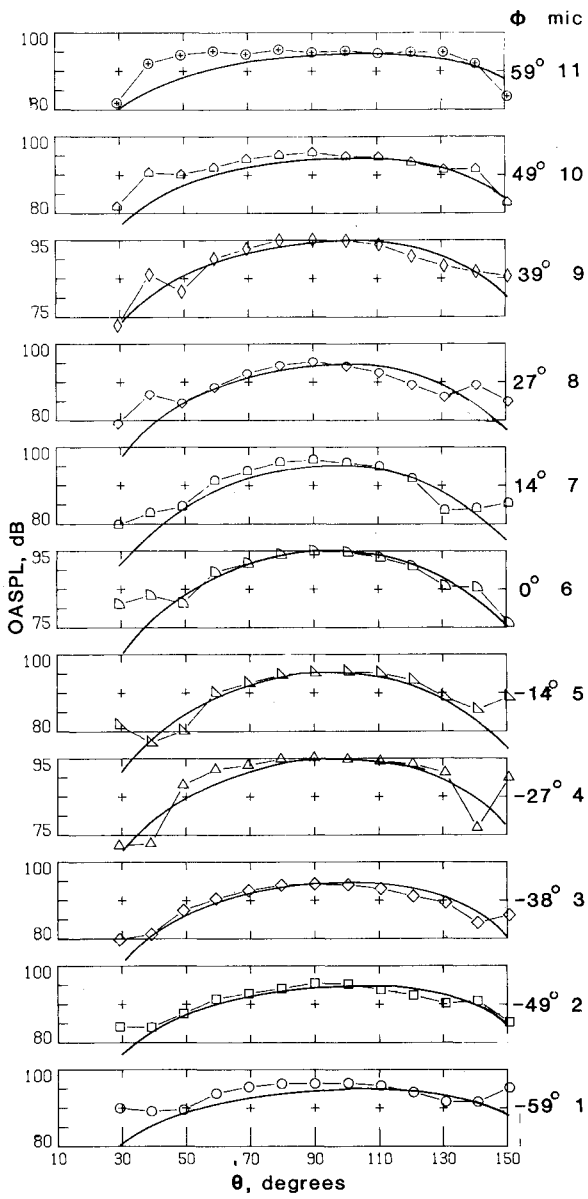

Fig. 7 Comparison of measured and predicted OASPL values normalized to a radius of 35 in. for an SRP tractor (run 53), noise level vs θ (symbols represent data levels, solid lines predicted levels).

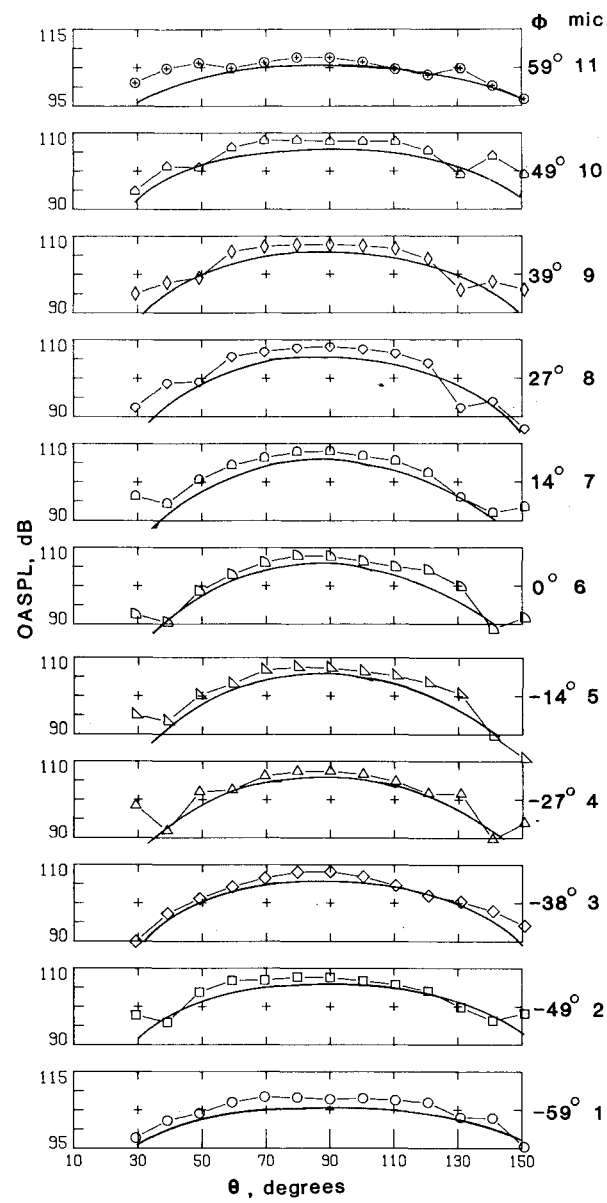

Fig. 8 Comparison of measured and predicted OASPL for run 54, noise level vs θ (symbols represent data levels, solid lines predicted levels).

for each of the harmonics is computed from these using

$$c_n = \{\bar{a}_n^2 + \bar{b}_n^2\}^{1/2}$$

and converted to decibels.

For ease of comparison and presentation, the data have been corrected to free-field levels by simply subtracting 6.02 dB from the measured levels. The free-field levels were then normalized to a constant radius of 35 in. from the propeller axis. This distance corresponded to the closest measurement point. The noise radiation pattern for selected configurations is presented in line contour plots with 5 dB intervals. Thus, these plots present the data corrected to free field, normalized to constant radius, and then displayed on the grid defined by the 143 microphone locations. To achieve a smooth representation for the contour plots, the 143 measurements were fit with a two-dimensional cubic spline having zero tension. Additional interpolated values were then calculated and the matrix of data was enriched from 11 (microphones) × 13 (streamwise stops) to a 50 × 50 matrix of evenly spaced points. These 50 points are indicated in the frame of the line contour plots.

Some comparisons are also presented in the coordinate system shown in Fig. 6. θ is the flyover angle defined between the flow vector and a line connecting the propeller disk axis to the center of the line of microphones (microphone 6) at a given streamwise stop. ϕ is the sideline angle defined between the vertical and the line of positions made by one microphone as it is traversed in the streamwise direction.

Results

Single-Rotation, Sting-Mounted Propeller

The sting-mounted SRP respresents the baseline or uninstalled configuration. Here the dominant noise levels are expected to arise from the blade thickness and steady loading, to have a azimuthal symmetry, and to be fairly well predicted by current propeller noise prediction techniques.[5,6]

A comparision of the data with the theory is presented in Fig. 7 for the low-tip-speed SRP tractor configuration (run 53) and in Fig. 8 for a high-tip-speed case (run 54). In these figures, the symbols represent the normalized data levels and the solid lines the predicted levels using only thickness and steady loading calculations. Each figure shows the variation

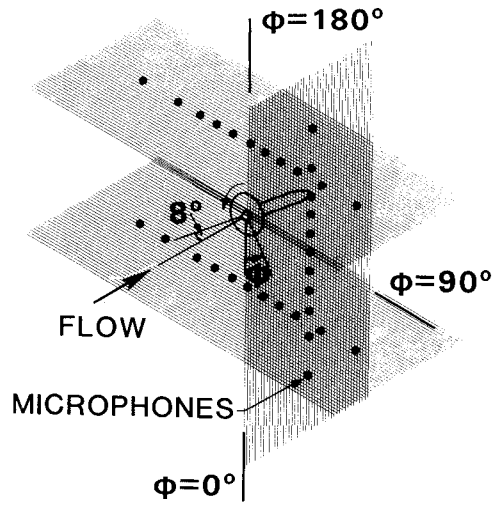

Fig. 9 Range over which noise data were obtained for propeller at nonzero angle of attack.

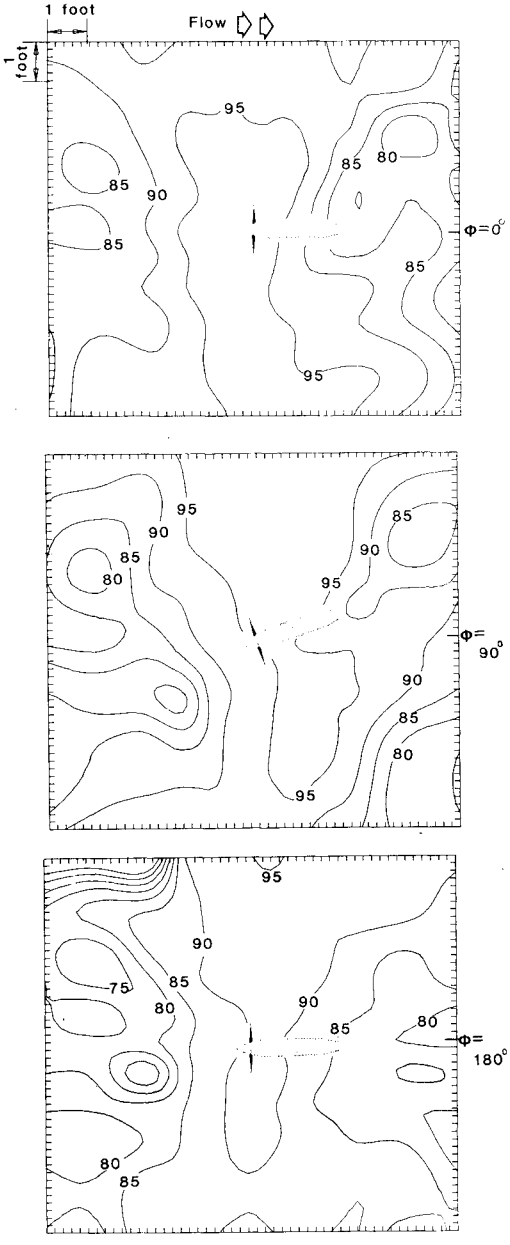

Fig. 10 Noise radiation pattern for SR-2 propeller at angle of attack (see Fig. 9) (values are in decibels).

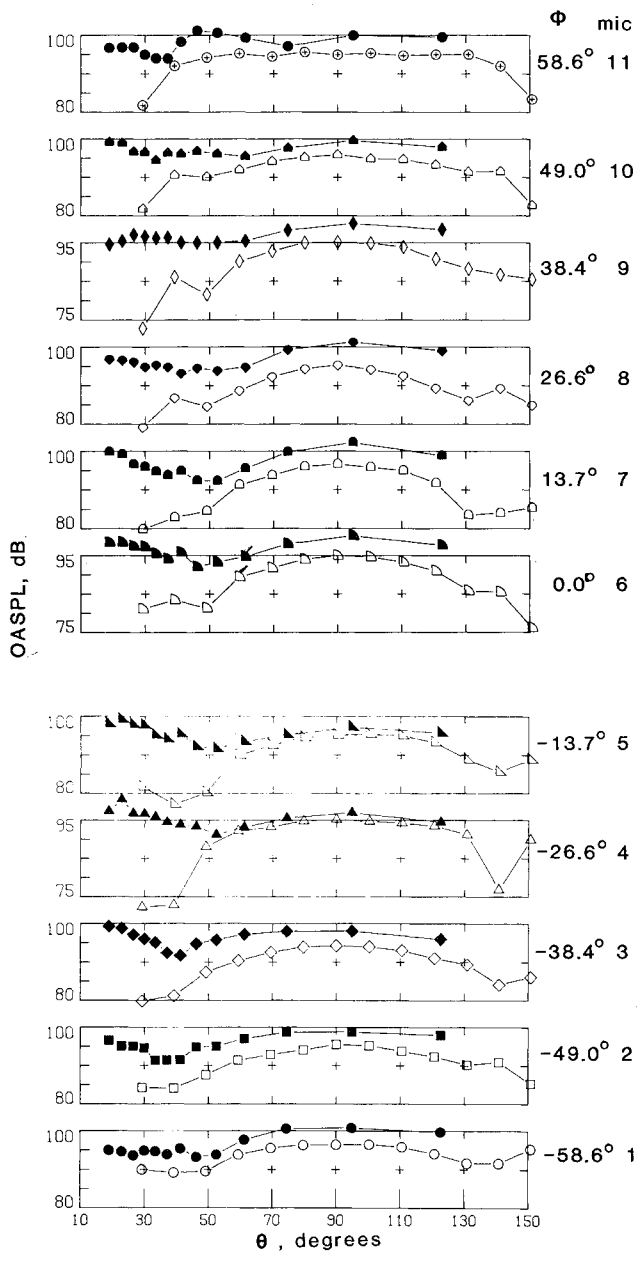

Fig. 11 Comparison of OASPL values for SR tractor (run 53, open symbols) and a pusher (run 135, solid symbols) propeller configurations vs flyover angle θ.

with the flyover angle θ. The comparisons show that for the low tip Mach number case (run 53, Fig. 7), the agreement between theory and experiment is excellent. Even in the regions where the background noise and propagation effects are producing data asymmetry, the data points are threaded by the theoretical values. The exceptions occur only at the extreme values of θ (29.3 and 150.7 deg), for which the data are underpredicted by as much as 10 dB. In these regions closer to the propeller axis, it is possible that nacelle diffraction and unsteadiness caused by variations in the blade setting and spacing may cause the higher noise levels. Also, unsteady loading may arise from the tunnel freestream turbulence (2%).

The data/theory comparisons for run 54 (high tip Mach number case) are shown in Fig. 8. The noise predictions indicate that the thickness noise is dominant for this propeller operation. The data trends are well predicted, with the levels being slightly underpredicted by about 2 dB. Again, only at the extreme values of θ are there large differences between the measured and predicted levels.

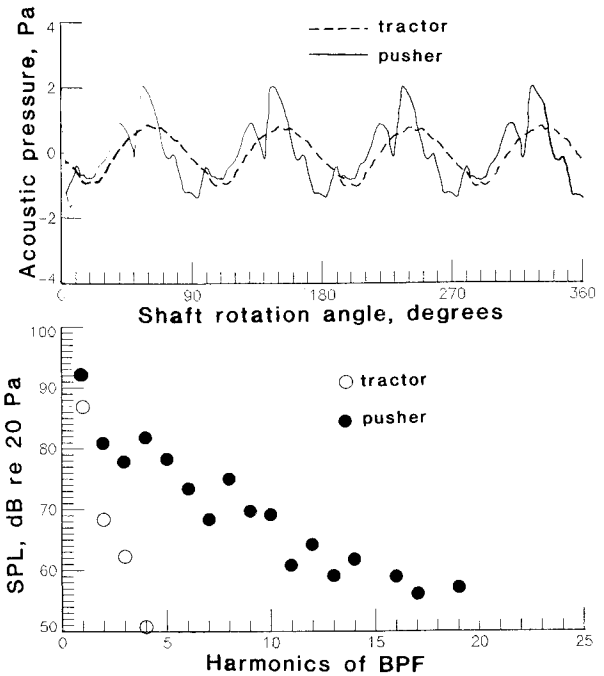

Fig. 12 Comparison of averaged pressure time history and spectrum from a tractor (run 53) and pusher (run 135) propeller operations.

Single-Rotation, Sting-Mounted Propeller at Nonzero Angle of Attack

The microphone carriage employed in this experiment allowed the noise radiation pattern to be measured to nominally 60 deg on either side of the vertical ($-60 < \phi < 60$ deg). An extended range of measurement locations was simulated by obtaining data for an angle of attack of -8 deg and noting that the relative geometry of the nacelle and microphone carriage at -8 deg was the same as if the nacelle had been left at $+8$ deg and the carriage rotated 180 deg about the tunnel centerline. In a like manner, yawing the nacelle was the equivalent to rotating the microphones through an angle of 90 deg. This procedure produced data extending from $\phi = -60$ to $+240$ deg, as illustrated in Fig. 9. Here $\phi = 0$ deg is the direction of a ground observer when the airplane is flying directly overhead at an angle of attack of 8 deg. The $\phi = 90$ deg direction corresponds to a sideline or fuselage observer and the data were actually obtained with the propeller axis yawed. The $\phi = 180$ deg direction corresponds to an observer above the aircraft and the data were obtained with the propeller axis at a pitch angle of -8 deg. Data were obtained at over 400 measurement positions for theory validation.[10] The measured results are shown in contour format in Fig. 10 for the low tip Mach number sequence of runs 64 (pitch angle of $+8$ deg), 151 (yaw angle of 10 deg), and 66 (pitch angle of -8 deg). The trends in the data indicate that the propeller noise has higher levels under the propeller ($\phi = 0$ deg) than above it ($\phi = 180$ deg). For this particular series, the difference in level from under to above the propeller is about 6 dB. These noise radiation trends were also observed for the other low tip Mach number sequence of runs (63, 150, and 65) for which the difference is about 8 dB, as well as the high tip Mach number sequences (67, 147, and 70; and 68, 148, and 69) where the difference is about 2 dB. The effect of angle of attack on the noise radiation pattern for the high tip Mach number cases is not as pronounced as for the higher loading (low tip Mach number) cases. However, these directivity patterns do display the rotation of the thickness noise component due to the rotation of the propeller disk.

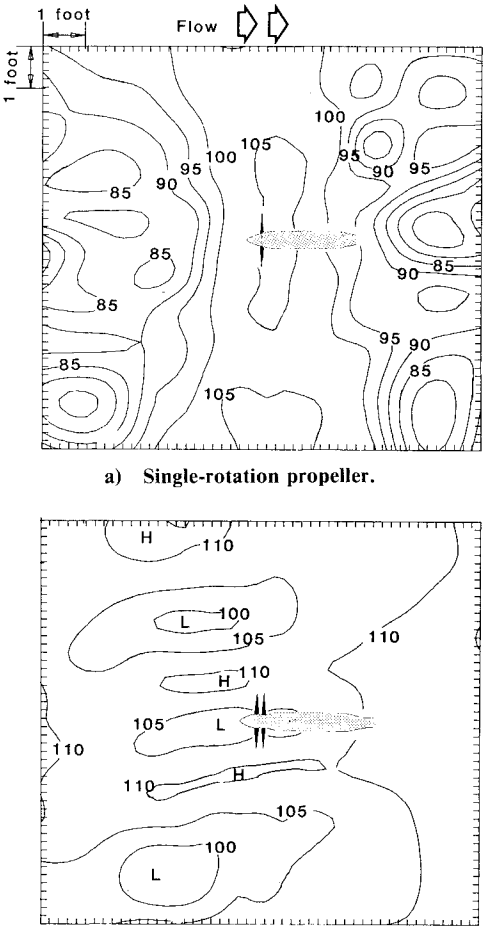

Fig. 13 Comparison of noise radiation patterns for eight-blade SRP and two four-blade CRPs (values are in decibels H = high, L = low).

Single-Rotation Propeller, Tractor vs Pusher Configuration

The effect on the noise radiation pattern of introducing a wake into an operating propeller is shown in Fig. 11. In this figure, the normalized overall sound pressure level (OASPL) is plotted against the flyover angle θ for the tractor (run 53 open symbols) and pusher operations (run 135, solid symbols). These are low tip Mach number cases. As expected, the pusher propeller produces higher noise levels than the tractor because of the unsteady loading introduced by the pylon wake. In the plane of the propeller ($\theta = 90$ deg), the difference in noise is 2-5dB. The largest differences are observed upstream of the propeller, where they are ~5-15+dB. These differences are smaller for the high tip Mach number cases for which the thickness sources dominate, but are larger for the other more lightly loaded low tip Mach number case (runs 52 and 134, not shown). This trend has been observed and reported previously[3] and stems from the fact that for lightly loaded propellers, the noise arising from the unsteady propeller loads exceeds that from the steady loads in certain directions.

The other effect of the pylon wake is on the noise signature from the propeller. In particular, spikes that give rise to higher levels of the higher harmonics are evident in the waveform.[7] An illustration of this change is shown in Fig. 12, where the average time history and average spectrum are presented for a tractor and a pusher installation. This sample was obtained from runs 53 and 135, microphone 6 (flagged symbols in Fig. 11). The changes in the pressure time history and spectrum are typical of all other microphone positions.

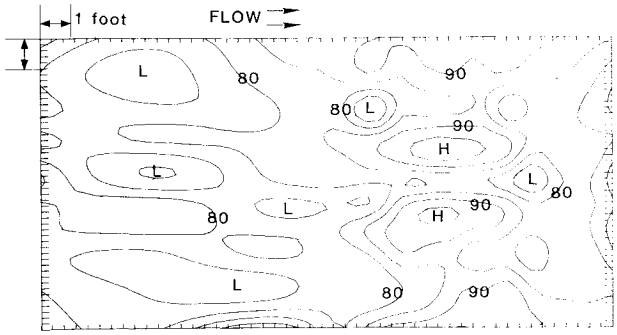

a) First harmonic.

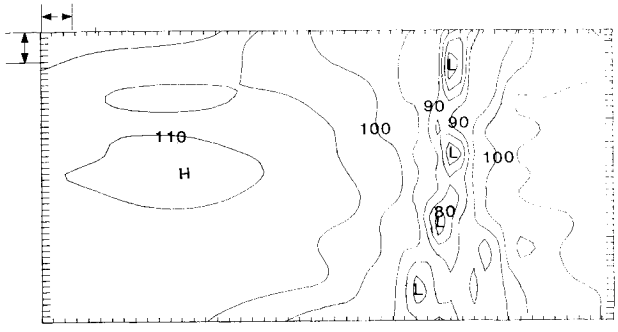

b) Second harmonic.

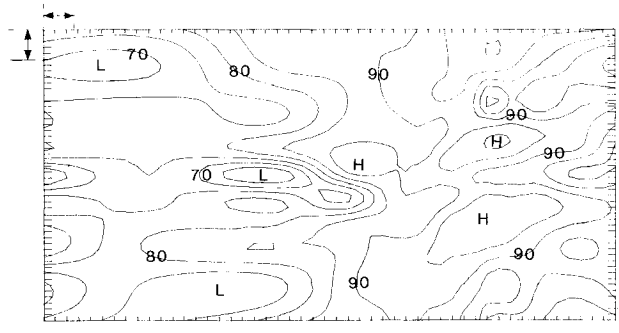

c) Third harmonic.

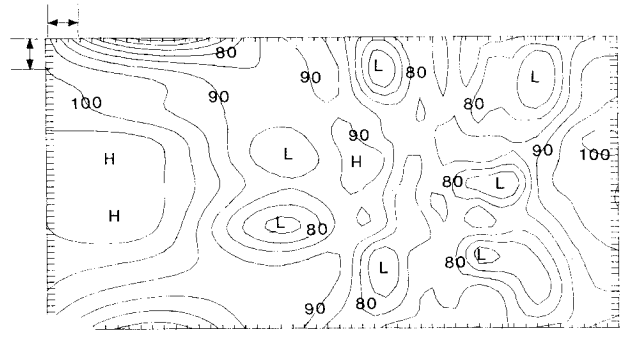

d) Fourth harmonic.

Fig. 14 Spatial distribution of the first four harmonics of the CR propeller noise (run 83).

Single-Rotation vs Counter-Rotation Propellers

A counter-rotation propeller is an extension of an SRP pusher installation, in that the second or aft propeller disk is encountering the wakes from the first. A comparison of the overall noise radiation patterns (OASPL) from an eight-blade SRP (run 141) and two counter-rotation, four-blade propellers (run 84) is shown in Fig. 13 in contour format for a high tip Mach number case. The SRP (Fig. 13a) has its maximum noise levels in the plane of the propeller disk. The noise levels decrease going upstream and downstream from the propeller disk. The noise pattern for the CRP is quite different. There are streamwise bands of alternating high and low noise levels repeating every 45 deg. These bands correspond to the directions in which the four blades from each disk are aligned or appear to "cross over" as they rotate 360 deg. The peak-to-peak levels in these bands are about 10 dB and are 5 dB higher and lower than those recorded for the eight-blade SRP. Another difference between the radiation patterns for the SRP and CRP is that the noise levels from the CRP increase upstream and downstream from the disk. This increase in the axial directions is similar to that observed for the pusher installation. In these directions, the CRP levels are about 30 dB higher than the SRP levels. The high CRP levels may arise from the fact that the blades are straight or unswept. In this situation, the blades on the aft disk encounter the entire wake shed from the front disk in a small instant of time. Also, with the same number of blades on each disk, these encounters occur at the same instant for all four blades.

Further insight into the CR noise sources is gained from the spatial distribution of each of the first four harmonics of the blade passage frequency of the noise from the CRP. These results are presented in Fig. 14 for the low tip Mach number case (run 83). Here the noise was also measured at two more positions upstream of the propeller. These positions correspond to $\theta = 12$ and 18 deg.

The data show that the second and fourth harmonics are the major contributors to the OASPL in the upstream and downstream directions. The second harmonic corresponds to the wake-cutting frequency and is thus attributed to the intradisk interactions, that is, the unsteady loads on the back disk produced by the front disk and vice versa. This interaction is expected to decrease with increased spacing between the propeller disks. It is also evident in Fig. 14 that the streamwise bands occurring at 45 deg intervals are the only noise patterns displayed in the first and third harmonics. This distribution of the harmonic levels was characteristic of all the CRP noise radiation patterns.

Conclusions

A movable microphone carriage permitted details of the noise radiation patterns to be measured for a representative set of SRP installations and for counter-rotation propellers. The baseline configuration results (the sting-mounted SR tractor) were used to validate the theory. The comparisons generally showed excellent agreement in both trends and noise levels. Measurements were made at a sufficiently large number (143) of microphone locations to validate the theory.

For a propeller at a nonzero angle of attack, the noise radiation patterns indicate that the noise levels decrease from under the propeller (ground observer, $\phi = 0$ deg) to above it ($\phi = 180$ deg). The difference in noise level between these two directions varied 2-8 dB, depending on the propeller operating conditions.

For a propeller in a pusher configuration, the changes in the noise characteristics from those of a tractor configuration are twofold. First, the noise radiation patterns show that the pusher is slightly noisier in the propeller plane (2-5 dB) and considerably noisier upstream (5-15 dB). The increase in noise level depends on the propeller operating conditions. Second, the wake introduces spikes into the pressure time history that produce higher noise levels in the higher harmonics. These spikes are evident at all microphone locations.

The noise radiation patterns for the CRP were quite different from those for the SRP. Streamwise bands of alternating high and low noise levels were observed in the directions corresponding to the blade alignments (every 45 deg for two four-blade CR propellers). In the lateral direction, the levels in these bands were 5 dB higher and 5 dB lower than the levels that were obtained for the eight-blade SRP. In addition, the CRP noise levels in the axial directions were about 30 dB higher than the SRP levels. Analysis of the harmonic contribu-

tions to the noise patterns indicates that the second and fourth harmonics give rise to the increased noise levels in the axial direction, whereas the first and third harmonics contain most of the noise energy in the streamwise bands. The high levels of interaction noise are attributed to the unswept propeller blade design coupled with the arrangement of the same number of blades on each disk.

References

[1]Tanna, H. K., Burrin, R. H., and Plumblee, H. E., Jr., "Installation Effects on Propeller Noise," *Journal of Aircraft,* Vol. 18, April 1981, pp. 303-309.

[2]Herkes, W., "An Experimental Study of the Noise by a Pusher Propeller Due to a Wake Entering the Propeller Disc," EOARD TR-80-5, Nov. 1979.

[3]Block, P. J. W., "Analysis of Noise Measured from a Propeller in a Wake," NASA TP-2358, 1984.

[4]Hubbard, H. H., "Sound from Dual-Rotating and Multiple Single-Rotating Propellers," NACA TN-1654, July 1948.

[5]Farassat, F., "Linear Acoustic Formulas for Calculation of Rotating Blade Noise," *AIAA Journal,* Vol. 19, Sept. 1981, pp. 1122-1130.

[6]Padula, S. L. and Block, P. J. W., "Acoustic Prediction Methods for the NASA Generalized Advanced Propeller Analysis System (GAPAS)," AIAA Paper 84-2243, July 1984.

[7]Block, P. J. W., "Installation Noise Measurements of Model SR and CR Propellers," NASA TM-85790, May 1984.

[8]Mitchell, G. A. and Mikkelson, D. C., "Summary and Recent Results from the NASA Advanced High-Speed Propeller Research Program," NASA TM-82891, 1983.

[9]Block, P. J. W. and Gentry, G. L., "Evaluation of the Langley 4-by 7-Meter Tunnel for Propeller Noise Measurements," NASA TM-85721, 1984.

[10]Padula, S. L. and Block, P. J. W., "Predicted Changes in Advanced Turboprop Noise with Shaft Angle-of-Attack," AIAA Paper 84-2346, 1984.